Inorg. Chem. **2005**, *44*, 2639–2646

Crystal Growth and Magnetic Properties of Lanthanide-Containing Osmium Double Perovskites, Ln_2NaOsO_6 (Ln = La, Pr, Nd)

William R. Gemmill,[†] Mark D. Smith,[†] Ruslan Prozorov,[‡] and Hans-Conrad zur Loye*[,†]

Department of Chemistry and Biochemistry, and Department of Physics & Astronomy, University of South Carolina, Columbia, South Carolina 29208

Received September 28, 2004

A series of double perovskite oxides, Ln_2NaOsO_6 (Ln = La, Pr, Nd), has been prepared as single crystals from acidic molten NaOH. All three oxides crystallize in the monoclinic space group $P2_1/n$ (Glazer tilt system #10, $a^-a^-b^+$), forming a 1:1 ordered rock salt lattice of the Na^+ and Os^{5+} cations. Magnetic susceptibility measurements show evidence of antiferromagnetic correlations in La_2NaOsO_6 and of a spin-flop transition from an antiferromagnetic to ferromagnetic-like state in both Pr_2NaOsO_6 and Nd_2NaOsO_6.

Introduction

Oxides of osmium are perhaps the least investigated of the platinum group metals, and only a limited number of compositions and structure types have been reported. Nonetheless, several interesting structures and properties have been found among the osmium oxides, including superconductivity in the recently reported KOs_2O_6 (T_c = 9.6 K)[1] and $RbOs_2O_6$ (T_c = 6.3 K)[2] and a metal−insulator transition (225 K) in $Cd_2Os_2O_7$.[3,4] In addition, although the number of osmates is quite limited, a reasonable variety of structures and compositions have been prepared, including several pyrochlores, $Cd_2Os_2O_7$,[3,4] $Tl_2Os_2O_7$,[5] $Hg_2Os_2O_7$,[6] $Ca_2Os_2O_7$,[7−9] $Ln_2Os_2O_7$ (Ln = Pr, Nd, Sm, Eu, Tb, Ho, Lu, Y),[10] simple perovskites, $AOsO_3$ (A = Ca, Sr, Ba),[8,11] and a number of other structure types and compositions, such as M_2OsO_3 (M = Li, Na),[12] $La_4Os_6O_{19}$,[13,14] $La_3Os_2O_{10}$,[15] $NdOsO_4$,[16] M_5OsO_6 (M = Li, Na),[17] Ln_3OsO_7 (Ln = La, Pr, Nd, Sm),[18,19] $MOsO_4$ (M = Na, K, Rb, Cs),[20] Cd_3OsO_6,[21] $Sr_{11}Os_4O_{24}$,[22] and MOs_2O_6 (M = K, Rb).[1]

Quaternary osmium-containing oxides are even less prevalent and include primarily double perovskites, such as Sr_2MOsO_6 (M = Li, Na, Mg, Ca, Sr, Fe, Co, Sc, Cr, In, Ga),[23] Ba_2MOsO_6 (M = Pr, Nd, Sm−Lu, Y),[24] Ba_2MOsO_6 (M = Co, Ni),[25] and Ba_2MOsO_6 (M = Li, Na),[23,26] and triple perovskites, such as $Ba_3MOs_2O_9$ (M = Li, Na).[27]

The vast majority of the above-mentioned compositions were prepared as polycrystalline powders, which is challenging because of the ease with which osmium picks up

* Author to whom correspondence should be addressed. E-mail: zurloye@sc.edu.
[†] Department of Chemistry and Biochemistry.
[‡] Department of Physics & Astronomy.

(1) Yonezawa, S.; Muraoka, Y.; Matsushita, Y.; Hiroi, Z. *J. Phys.: Condens. Matter* **2004**, *16*, L9.
(2) Yonezawa, S.; Muraoka, Y.; Matsushita, Y.; Hiroi, Z. *J. Phys. Soc. Jpn.* **2004**, *74*, 819.
(3) Reading, J.; Weller, M. T. *J. Mater. Chem.* **2001**, *11*, 2373.
(4) Sleight, A. W.; Gillson, J. L.; Weiher, J. F.; Bindloss, W. *Solid State Commun.* **1974**, *14*, 357.
(5) Sleight, A. W.; Gillson, J. L. *Mater. Res. Bull.* **1971**, *6*, 781.
(6) Reading, J.; Gordeev, S.; Weller, M. T. *J. Mater. Chem.* **2002**, *12*, 646.
(7) Shaplygin, I. S.; Lazarev, V. B. *Thermochim. Acta* **1977**, *20*, 381.
(8) Chamberland, B. L. *Mater. Res. Bull.* **1978**, *13*, 1273.
(9) Reading, J.; Knee, C. S.; Weller, M. T. *J. Mater. Chem.* **2002**, *12*, 2376.
(10) Shaplygin, I. S.; Lazarev, V. B. *Mater. Res. Bull.* **1973**, *8*, 761.
(11) Shaplygin, I. S.; Lazarev, V. B. *Russ. J. Inorg. Chem.* **1976**, *21*, 1279.
(12) Lazarev, V. B.; Shaplygin, I. S. *Russ. J. Inorg. Chem.* **1978**, *23*, 802.
(13) Shaplygin, I. S.; Lazarev, V. B. *Dokl. Akad. Nauk SSSR* **1978**, *241*, 420.
(14) Abraham, F.; Trehoux, J.; Thomas, D. *Mater. Res. Bull.* **1977**, *12*, 43.
(15) Abraham, F.; Trehoux, J.; Thomas, D. *J. Solid State Chem.* **1979**, *29*, 73.
(16) Abraham, F.; Trehoux, J.; Thomas, D. *J. Inorg. Nucl. Chem.* **1980**, *42*, 1627.
(17) Betz, T.; Hoppe, R. *Z. Anorg. Allg. Chem.* **1985**, *524*, 17.
(18) Lam, R.; Wiss, F.; Greedan, J. E. *J. Solid State Chem.* **2002**, *167*, 182.
(19) Plaisier, J. R.; Drost, R. J.; IJdo, D. J. W. *J. Solid State Chem.* **2002**, *169*, 189.
(20) Levason, W.; Tajik, M.; Webster, M. *J. Chem. Soc., Dalton Trans.* **1985**, 1735.
(21) Lazarev, V. B.; Shaplygin, I. S. *Russ. J. Inorg. Chem.* **1979**, *24*, 128.
(22) Tomaszewska, A.; Müller-Buschbaum, H. *Z. Anorg. Allg. Chem.* **1993**, *619*, 1738.
(23) Sleight, A. W.; Longo, J.; Ward, R. *Inorg. Chem.* **1962**, *1*, 245.
(24) Treiber, V. U.; Kemmler-Sack, S. *Z. Anorg. Allg. Chem.* **1981**, *478*, 223.
(25) Treiber, V. U.; Kemmler-Sack, S. *Z. Anorg. Allg. Chem.* **1980**, *470*, 95.
(26) Stitzer, K. S.; Smith, M. D.; zur Loye, H.-C. *Solid State Sci.* **2002**, *4*, 311.
(27) Stitzer, K. S.; El Abed, A.; Smith, M. D.; Davis, M. J.; Kim, S.-J.; Darriet, J.; zur Loye, H.-C. *Inorg. Chem.* **2003**, *42*, 947.

10.1021/ic048637x CCC: $30.25 © 2005 American Chemical Society
Published on Web 03/03/2005

oxygen; only a few select compositions have been prepared as single crystals. Our group has focused on the single-crystal growth of lanthanide-containing oxides of platinum group metals in an effort to investigate both the structural chemistry and the magnetic properties of platinum group metal oxides. To that effect, we have recently developed a procedure using molten hydroxides fluxes to grow single crystals of complex osmium oxides, including Ba_2MOsO_6 (M = Li, Na)[26] and $Ba_3MOs_2O_9$ (M = Li, Na).[27] The acid−base chemistry of hydroxide fluxes, described by the Lux−Flood acid−base definition,[28,29] allows for a wide range of species to be present in solution, an essential prerequisite for their incorporation into single crystals. In addition, it is known that molten hydroxides are an excellent solvent of crystallization for lanthanide-containing oxides,[30,31] where the solubility of the lanthanides is dictated by the acid−base properties of the melt. Specifically, the water content of the melt must be controlled to enable the dissolution of the lanthanide oxides (Ln_2O_3's),[28,29,32] which are only soluble in acidic "wet" melts.[31] We have recently shown that such "wet" melts are one route for the growth of oxide single crystals containing both lanthanide and platinum group metals.[33−35] Using this method, we have been successful in preparing a series of new double perovskites of the general formula Ln_2NaMO_6 (Ln = La, Pr, Nd; M = Ir,[36] Ru[34]). This paper reports an extension of this work to the osmium analogues, Ln_2NaOsO_6 (Ln = La, Pr, Nd); the crystal growth, structural characterization, and magnetic properties of these new double perovskites are discussed herein.

Experimental Section

Crystal Growth. In a 1:1 molar ratio of Os:Ln_2O_3, 1 mmol of Os powder (J & J Materials, Inc., 99.98%), 1 mmol of Ln_2O_3 (Ln = La, Nd) (activated by heating the oxide from the bottle (Alfa, 99.9%) in air at 1000 °C for 12 h) or Pr_2O_3 (prepared by heating $Pr(OH)_3$ in a 5%/95% H_2/N_2 atmosphere at 1000 °C for 24 h), NaOH (4.08 g, 102 mmol; Fisher, reagent grade), and 1 g of H_2O were added to a silver tube 0.5" in diameter that had been flame sealed at one end and securely crimped shut on the other end. The reaction mixture was heated at a rate of 10 °C/min to 600 °C, held at temperature for 24 h, and then quickly cooled to room temperature by turning off the furnace. The crystals were removed from the flux by washing with water, aided by the use of sonication.

Single-Crystal X-ray Diffraction. For the structure determination of La_2NaOsO_6, Pr_2NaOsO_6, and Nd_2NaOsO_6, black crystals were mounted onto the end of thin glass fibers. X-ray intensity data were measured at 293(2) K on a Bruker SMART APEX diffractometer (Mo Kα radiation, $\lambda = 0.71073$ Å) for Ln_2NaOsO_6 (Ln = La, Nd) and at 294(2) K for Pr_2NaOsO_6. The data collection covered 99.5% of reciprocal space to $2\theta = 65.2°$ (average redundancy = 4.1) for La_2NaOsO_6, 99.5% of reciprocal space to $2\theta = 70.2°$ (average redundancy = 3.8) for Pr_2NaOsO_6, and 99.5% of reciprocal space to $2\theta = 72.4°$ (average redundancy = 3.6) for Nd_2NaOsO_6. Raw area detector data frame integration and Lp corrections were carried out with SAINT+.[37] Final unit cell parameters were determined by least-squares refinement of all reflections with $I > 5\sigma(I)$ from each data set (2930 for La_2NaOsO_6, 3378 for Pr_2NaOsO_6, and 3198 for Nd_2NaOsO_6). Analysis of each data set showed negligible crystal decay during data collection. The data were corrected for absorption effects with SADABS.[37]

Table 1. Crystal Data and Structural Refinement for Ln_2NaOsO_6 (Ln = La, Pr, Nd)

empirical formula	La_2NaOsO_6	Pr_2NaOsO_6	Nd_2NaOsO_6
formula weight (g/mol)	587.01	591.01	597.67
space group	$P2_1/n$	$P2_1/n$	$P2_1/n$
unit cell dimensions			
a (Å)	5.6054(3)	5.5427(2)	5.5162(2)
b (Å)	5.9445(3)	5.9289(2)	5.9189(2)
c (Å)	8.0085(4)	7.9509(3)	7.9293(3)
b	90.587(2)°	90.854(1)°	90.987(1)°
V (Å^3)	267.51(2)	261.254(16)	255.852(16)
Z	2	2	2
density (calculated) (Mg m^{-3})	7.288	7.513	7.668
absorption coefficient (mm^{-1})	39.409	42.649	44.281
reflections collected	4094	4491	4659
independent reflections	969 (R_{int} = 0.0334)	1147 (R_{int} = 0.0259)	1252 (R_{int} = 0.0319)
GOF on F^2	1.146	1.143	1.110
final R indices [$I > 2\sigma(I)$]	R1 = 0.0234, wR2 = 0.0514	R1 = 0.0231, wR2 = 0.0472	R1 = 0.0271, wR2 = 0.0516
R indices (all data)	R1 = 0.0258, wR2 = 0.0525	R1 = 0.0262, wR2 = 0.0483	R1 = 0.0311, wR2 = 0.0528
extinction coefficient	0.0180(7)	0.0076(3)	0.0043(3)
residual electron density (e Å^{-3})	2.748 and −2.209	2.865 and −2.567	2.585 and −2.047

The compounds Ln_2NaOsO_6 (Ln = La, Pr, Nd) crystallize with monoclinic symmetry in the space group $P2_1/n$ as determined by the pattern of systematic absences in the intensity data. The structures were solved by a combination of direct methods and difference Fourier syntheses and were refined by full-matrix least-squares against F^2, with SHELXTL.[38] Refinement of the site occupation factors for the metal atoms showed no significant deviation from full occupancy in either case.

Due to the monoclinic β angles of 90.587(2)°, 90.854(1)°, and 90.987(1)° for La_2NaOsO_6, Pr_2NaOsO_6, and Nd_2NaOsO_6, respectively, a check for pseudo-orthorhombic twinning was performed by including the twin matrix [100/0−10/00−1] in a refinement cycle. The refined twin fractions (SHELX BASF parameter) were 1.00/0.0 in each case, indicating genuine single crystals. The twin matrix was not included in the final cycles. Relevant crystallographic data from the single-crystal structure refinements for the compounds Ln_2NaOsO_6 (Ln = La, Pr, Nd) are compiled in Table 1. For all three compounds, atomic positions and selected inter-

(28) Flood, H.; Forland, T. *Acta Chem. Scand.* **1947**, *1*, 592.
(29) Lux, H. *Elektrochem.* **1939**, *45*, 303.
(30) Luce, J. L.; Stacy, A. M. *Chem. Mater.* **1997**, *9*, 1508.
(31) Keller, S. W.; Carlson, V. A.; Sanford, D.; Stenzer, F.; Stacy, A. M.; Kwei, G. H.; Alario-Franco, M. *J. Am. Chem. Soc.* **1994**, *116*, 8070.
(32) Goret, J. *Bull. Soc. Chim.* **1964**, 1074.
(33) Davis, M. J.; Smith, M. D.; zur Loye, H.-C. *Inorg. Chem.* **2003**, *42*, 6980.
(34) Gemmill, W. R.; Smith, M. D.; zur Loye, H.-C. *J. Solid State Chem.* **2004**, *177*, 3560.
(35) Gemmill, W. R.; Smith, M. D.; zur Loye, H.-C. *Inorg. Chem.* **2004**, *43*, 4254.
(36) Davis, M. J.; Mugavero, S. J.; Glab, K. I.; Smith, M. D.; zur Loye, H.-C. *Solid State Sci.* **2004**, *5*, 413.
(37) *SMART Version 5.625, S. V., and SADABS Version 2.05*; Bruker Analytical X-ray Systems, Inc.: Madison, WI, 2001.
(38) Sheldrick, G. M. *SHELXTL*; Bruker Analytical X-ray Systems, Inc.: Madison, WI, 1997.

Table 2. Atomic Coordinates and Equivalent Isotropic Displacement Parameters for La_2NaOsO_6, Pr_2NaOsO_6, and Nd_2NaOsO_6

	x	y	z	*U*(eq)
		La_2NaOsO_6		
La	0.4839(1)	0.0644(1)	0.2519(1)	0.006(1)
Na	0	0	0	0.008(1)
Os	$^1/_2$	$^1/_2$	0	0.004(1)
O1	0.2126(7)	0.3237(7)	0.0479(4)	0.007(1)
O2	0.6050(7)	0.4587(7)	0.2306(5)	0.009(1)
O3	0.3309(7)	0.7788(7)	0.0598(5)	0.009(1)
		Pr_2NaOsO_6		
Pr	0.4815(1)	0.0687(1)	0.2528(1)	0.007(1)
Na	0	0	0	0.004(1)
Os	$^1/_2$	$^1/_2$	0	0.008(1)
O1	0.2078(6)	0.3272(6)	0.0508(4)	0.008(1)
O2	0.6161(7)	0.4502(7)	0.2318(5)	0.009(1)
O3	0.3363(6)	0.7809(7)	0.0674(5)	0.009(1)
		Nd_2NaOsO_6		
Nd	0.4805(1)	0.0700(1)	0.2530(1)	0.007(1)
Na	0	0	0	0.006(1)
Os	$^1/_2$	$^1/_2$	0	0.005(1)
O1	0.2070(7)	0.3237(7)	0.0514(5)	0.009(1)
O2	0.6181(7)	0.4587(7)	0.2309(5)	0.009(1)
O3	0.3373(7)	0.7805(7)	0.0680(5)	0.010(1)

Table 3. Selected Interatomic Distances (Å), Bond Angles (deg), and Tolerance Factors for La_2NaOsO_6, Pr_2NaOsO_6, and Nd_2NaOsO_6

	La_2NaOsO_6	Pr_2NaOsO_6	Nd_2NaOsO_6
Ln−O(1)	2.425(4)	2.374(4)	2.365(4)
	2.705(4)	2.675(4)	2.659(4)
	2.770(4)	2.735(4)	2.725(4)
Ln−O(2)	2.391(4)	2.340(4)	2.329(4)
	2.447(4)	2.388(4)	2.374(4)
Ln−O(3)	2.443(4)	2.387(4)	2.382(4)
	2.661(4)	2.608(4)	2.593(4)
	2.871(4)	2.894(4)	2.891(4)
Na−O(1) (×2)	2.294(4)	2.289(4)	2.284(4)
Na−O(2) (×2)	2.260(4)	2.256(4)	2.262(4)
Na−O(3) (×2)	2.320(4)	2.328(4)	2.325(4)
Os−O (×2)	1.963(4)	1.964(4)	1.961(4)
Os−O (×2)	1.953(4)	1.965(4)	1.957(4)
Os−O (×2)	1.971(4)	1.974(4)	1.967(4)
Os−O(1)−Na	147.2(2)	145.10(18)	144.8(2)
Os−O(2)−Na	144.5(2)	140.6(2)	139.9(2)
Os−O(3)−Na	144.26(19)	141.06(19)	140.8(2)
t	0.89	0.88[a]	0.86

[a] The ionic radius for Pr^{3+} in CN-12 was obtained through a linear fit extrapolation of known lanthanide element values.[46]

atomic distances and angles are summarized in Tables 2 and 3, respectively.

Scanning Electron Microscopy. Environmental scanning electron micrographs (ESEM) of several single crystals were obtained using a FEI Quanta 200 ESEM instrument utilized in the low vacuum mode. ESEM images of Pr_2NaOsO_6 and Nd_2NaOsO_6 are shown in Figure 2a and b, respectively. The ESEM also verified the presence of sodium, osmium, and oxygen for all samples and lanthanum, praseodymium, and neodymium for La_2NaOsO_6, Pr_2NaOsO_6, and Nd_2NaOsO_6, respectively. Furthermore, within the detection limits of the instrument, it demonstrated the absence of other elements in the crystals.

Magnetic Susceptibility. The magnetic susceptibility of the compounds Ln_2NaOsO_6 (Ln = La, Pr, Nd) was measured using a Quantum Design MPMS XL SQUID magnetometer. For the magnetic measurements, loose crystals of Ln_2NaOsO_6 (Ln = La, Pr, Nd) were placed into gelatin capsules, which were placed inside plastic straws. Samples were measured under both zero-field-cooled (ZFC) and field-cooled (FC) conditions. For all measurements, the total magnetic moment was measured in the temperature range of 2−300 K. Measurements were carried out in applied fields ranging from 1 to 40 kG. In addition, field sweeps were recorded between +40 and −40 kG at 100 and 2 K for La_2NaOsO_6 and Pr_2NaOsO_6 and at 2, 10, 20, and 100 K for Nd_2NaOsO_6. The very small diamagnetic contribution ($\sim 10^{-6}$ emu) of the gelatin capsule containing the sample had a negligible contribution to the overall magnetization, which was dominated by the sample signal.

Figure 1. Crystal structure of Ln_2NaOsO_6 (Ln = La, Pr, Nd); OsO_6 octahedra are shown in orange, NaO_6 octahedra are purple, and the black spheres represent Ln^{3+} cations.

Results and Discussion

Perovskite oxides are perhaps the most studied family of compounds in solid-state chemistry due to their inherent ability to accommodate a wide range of elemental compositions and to display a wealth of structural variations. Perovskites have the general formula ABO_3, where A typically represents a large electropositive cation and B represents a smaller transition metal or main group ion. In its ideal form, the cubic ABO_3 perovskite can be described as consisting of corner-sharing BO_6 octahedra with the A cation occupying the 12-fold coordination site in the center of eight such octahedra. The ideal double perovskite structure of the general formula $A_2BB'O_6$ is obtained when the B cation is substituted by a B′ cation in an ordered 1:1 fashion, doubling the unit cell. The B(B′) cation distribution in the 1:1 ordered system can exist in either a rock salt or a layered fashion, the former being the most common[39,40] (Figure 1). The structures of La_2NaOsO_6, Pr_2NaOsO_6, and Nd_2NaOsO_6, discussed below, form in the monoclinic distortion of the double perovskite structure.

Crystal Structures. Small black crystals of La_2NaOsO_6, Pr_2NaOsO_6, and Nd_2NaOsO_6 were grown from molten hydroxide fluxes in which the flux acted as both a solvent and a reactant. Figure 2a and b shows ESEM images of flux

(39) Anderson, M. T.; Greenwood, K. B.; Taylor, G. A.; Poeppelmeier, K. R. *Prog. Solid State Chem.* **1993**, *22*, 197.
(40) Mitchell, R. M. *Perovskites: Modern and Ancient*; Almaz Press: Thunder Bay, 2002.

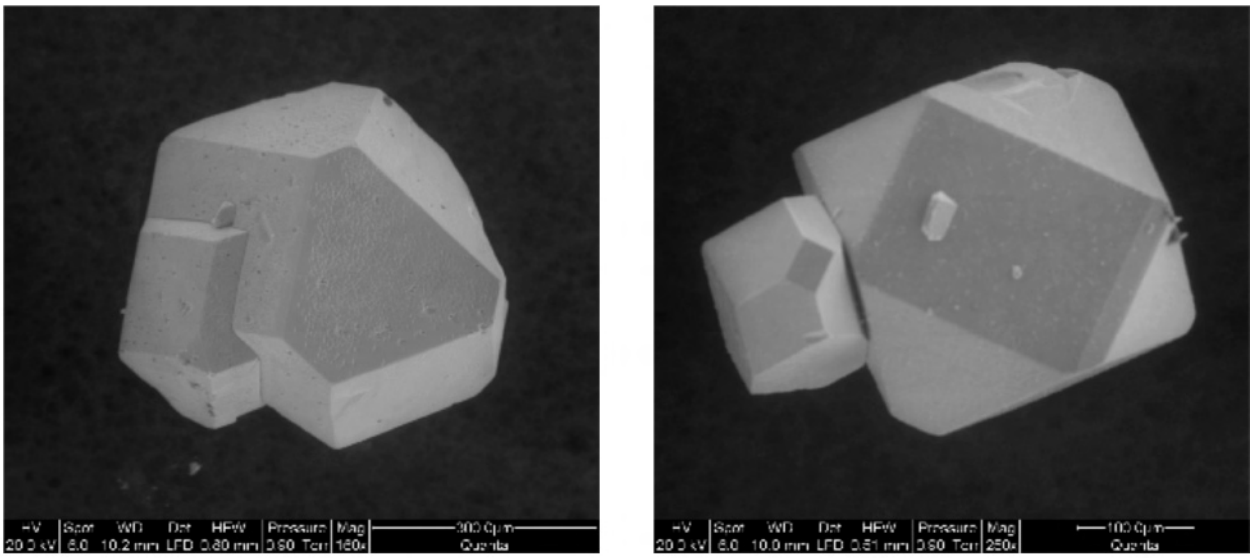

Figure 2. ESEM images of flux grown crystals of (a) Pr_2NaOsO_6 and (b) Nd_2NaOsO_6. Both crystals measure approximately 200 μm on edge.

grown crystals of Pr_2NaOsO_6 and Nd_2NaOsO_6, respectively, illustrating the growth morphology, which is representative for crystals of this structure type, for example, Nd_2NaIrO_6[36] and Nd_2NaRuO_6.[34]

The title compounds Ln_2NaOsO_6 (Ln = La, Pr, Nd) crystallize in the space group $P2_1/n$, with the monoclinic-distorted double perovskite structure type. This space group allows for a 1:1 ordered arrangement of the B and B′ cations in a rock-salt type lattice and the tilting of the BO_6 and $B'O_6$ octahedra to accommodate the small size of the A cation. The Glazer tilt system assigned to the $P2_1/n$ space group is #10, $a^-a^-b^+$.[41−43] [This notation ($a^0b^0c^0$) refers to both the magnitude (the letter) and the phase (the sign of the superscript) of the tilts about the *a*, *b*, and *c* axes, respectively.] In the title compounds, the Na^+ and Os^{5+} cations lie on the two crystallographically independent octahedral sites, while the Ln^{3+} cations occupy the A site in an 8-fold coordination environment.

It is known that osmium can be stabilized in the B-site of the double perovskite structure type. The reported double perovskites of osmium furthermore demonstrate that osmium can be stabilized in a variety of oxidation states ranging from +7 to +5 as exemplified by the following compositions, $Ba_2MOs^{VII}O_6$ (M = Li, Na),[23,26] $Ba_2MOs^{VI}O_6$ (M = Co, Ni),[25] and $Ba_2MOs^{V}O_6$ (M = Pr, Nd, Sm−Lu, Y).[24] Another possible composition for which osmium would be pentavalent is Ln_2MOsO_6 (Ln = lanthanide, M = alkali metal); the title compounds Ln_2NaOsO_6 (Ln = La, Pr, Nd) belong to this subset.

A comparison of bond distances for La_2NaOsO_6, Pr_2NaOsO_6, and Nd_2NaOsO_6 shows that they fall within the accepted ranges. Specifically, the Os−O bond distances in Ln_2NaOsO_6 (Ln = La, Pr, Nd) range from 1.953(4) to 1.974(4) Å and are consistent with the values observed in other Os(V) oxides with this structure type and other structures with pentavalent osmium.[6,24] The Na−O distances in Ln_2NaOsO_6 (Ln = La, Pr, Nd) range from 2.260(4) to 2.328(4) Å and are typical for Na^+ in an octahedral environment within the double perovskite structure type.[26,34,36]

The distortion from the ideal cubic double perovskite structure for the compositions discussed in this paper is a result of the tilting of the NaO_6 and OsO_6 octahedra, while maintaining their corner-sharing connectivity. This is commonly observed for compositions that include an A cation that is too small to fill the 12-fold coordination site and results in a reduced 8-fold coordination environment for the A cation in the monoclinic structure. As both the A−O and the B−O bond lengths are limited to a narrow range, the Na−O−Os bond angles must distort. The smaller is the A cation, the greater is the degree of distortion of the Na−O−Os bond angle away from the ideal 180°; consequently, the β angle of the monoclinic unit cell can be considered a measure of the structure distortion. In the case of the title compounds, the β angle increases with decreasing size of the A cation, concomitantly with an increase in the deviation from the ideal 180° Na−O−Os bond angles, as shown in Tables 1 and 3, respectively. This feature of rotated octahedra, common among all $P2_1/n$ ordered double perovskites, requires that the BO_6 and $B'O_6$ octahedra have different tilt angles as a result of the differences in size and distortion of each of the two polyhedron. These tilt angles can be calculated using a set of equations derived by Groen et al. from the cell parameters and atomic coordinates.[44] An alternative method of determining the tilt angles for the MO_6 and $M'O_6$ octahedra is based on the atomic coordinates and the average M−O bond distances and can be generated from the Tilting Using Backward Equations Relationship Software

(41) Woodward, P. M. *Acta Crystallogr.* **1997**, *B53*, 44.
(42) Woodward, P. M. *Acta Crystallogr.* **1997**, *B53*, 32.
(43) Glazer, A. M. *Acta Crystallogr.* **1972**, *B28*, 3384.
(44) Groen, W. A.; van Berkel, F. P. F.; IJdo, D. J. W. *Acta Crystallogr.* **1986**, *C42*, 1472.

Table 4. Octahedral Tilt Angles Calculated from the Tilting Using Backward Equations Relationship Software (TUBERS) Program Associated with SPuDS[24]

	octahedral tilt angles	
compound	NaO_6	OsO_6
La_2NaOsO_6	17.6°	21.0°
Pr_2NaOsO_6	18.6°	22.1°
Nd_2NaOsO_6	18.9°	22.6°

(TUBERS) program associated with the Structure Prediction Diagnostic Software (SPuDS).[45] These angles are listed in Table 4. Figure 3 shows the variation of the lattice parameters and β angle as a function of Ln^{3+} size for the three series of double perovskites Ln_2NaMO_6 (Ln = La, Pr, Nd; M = Ru, Ir, and Os).[34,36] One can observe clear trends as a function of rare earth size in the lattice parameters for the ruthenium, iridium, and osmium series. The iridium series deviates at times from the trend set by the ruthenium and osmium series, for example, in the *c*-parameter and β-angle; nonetheless, the values are all tightly clustered, which is expected on the basis of the almost identical ionic radii of Ir^{5+}, Ru^{5+}, and Os^{5+} of 0.570, 0.565, and 0.575 Å, respectively.[46]

In related double perovskites, Ln_2NaIrO_6 (Ln = La, Pr, Nd)[36] and Ln_2NaRuO_6 (Ln = La, Pr, Nd),[34] it was observed that no lanthanide cations smaller than Sm^{3+} could be stabilized in the double perovskite structure. The same holds true for the Ln_2NaOsO_6 (Ln = La, Pr, Nd) system reported herein. This limitation can be understood when looking at the Goldschmidt tolerance factor, *t*, which quantifies the relationship between the radii of the ions and the stability of the perovskite structure.[47] As in the case of the series Ln_2NaIrO_6 (Ln = La, Pr, Nd)[36] and Ln_2NaRuO_6 (Ln = La, Pr, Nd),[34] the Sm_2NaOsO_6 analogue would possess a tolerance factor smaller than 0.86, which appears to be the approximate lower limit for these Ln_2NaMO_6 double perovskite series. This is also supported by the global instability index (GII) given in the Structure Prediction Diagnostic Software (SPuDS), which reaches a value of >0.1 for the compositions Ln_2NaOsO_6 (Ln = Sm−Lu), indicating that the probability of their formation is unfavorable.[45] Experimentally we have observed that in hydroxide fluxes the smaller lanthanides samarium, europium, and gadolinium react with osmium to form the fluorite-related oxide phases Ln_3OsO_7 (Ln = Sm, Eu, Gd).[48]

Magnetism. La_2NaOsO_6. The temperature dependence of the magnetization for La_2NaOsO_6 in applied fields of 1, 10, and 20 kG is shown in Figure 4. Fitting the high-temperature susceptibility ($100 < T < 300$) to the Curie−Weiss law, given by

$$\chi_{cw} = C/(T - \theta)$$

where C is the Curie constant, and θ is the Curie−Weiss temperature, results in values of $\mu_{eff} = 3.26\ \mu_B$, $C = 1.33$ emu/K mol^{-1}, $\theta = -74$ K, which is lower than the theoretical spin-only value for d^3 Os(V) cation of 3.87 μ_B, as expected for Os(V) due to the presence of spin−orbit coupling.[19] While the negative Weiss constant is indicative of antiferromagnetic correlations, the plot of the magnetization as a function of temperature shows a sudden upturn at about 17 K, which may indicate the onset of a canted antiferromagnetic state. As trivalent lanthanum is a nonmagnetic cation, this represents the magnetic behavior of Os(V) d^3 in this structure type. The magnetic field dependence of the magnetization was recorded at both 100 and 2 K and showed paramagnetic behavior at 100 K. At 2 K, the magnetization versus field plot is nonlinear and exhibits a small hysteresis at 2 K, consistent with the proposed canted antiferromagnetic state, Figure 5.

Pr_2NaOsO_6. The temperature dependence of the magnetization of Pr_2NaOsO_6 measured in applied fields of 1, 10, 20, and 40 kG is shown in Figure 6. At first glance, this plot is similar to Figure 4, although a slight downturn in the magnetization at 7 K is observed in the 10 kG data set, suggesting the existence of antiferromagnetic correlations. Fitting the high-temperature susceptibility ($100 < T < 300$) to the Curie−Weiss law (see above) results in values of $\mu_{eff} = 6.28\ \mu_B$, $C = 4.95$ emu/K mol^{-1}, $\theta = -10$ K, which is in good agreement with the theoretical value (6.37 μ_B). The theoretical moment is calculated by taking the square root of the sum of the squares of the moments of the contributing magnetic cations, $\mu_{eff} = \sqrt{(\mu_B Pr^{3+})^2 + (\mu_B Pr^{3+})^2 + (\mu_B Os^{5+})^2} = \sqrt{(3.58)^2 + (3.58)^2 + (3.87)^2} = 6.37\ \mu_B$. However, if the theoretical moment is calculated using the magnetic moment of Os(V) determined from La_2NaOsO_6 ($\mu_{eff} = 3.26$), a value of 6.02 μ_B is obtained instead, worsening the agreement.

The Weiss constant is negative (−10 K), again providing evidence for net antiferromagnetic correlations. The magnetization, however, is field dependent at low temperatures. Figure 7 shows the field dependence of the magnetization recorded at 100 and 2 K. At 100 K, the plot is linear, indicating paramagnetic behavior. At 2 K, the magnetization curve exhibits a noticeable increase above 10 kG, which can be attributed to a transition from an antiferromagnetic to a spin-flop state. The Weiss constant (−10 K) is less negative than that of La_2NaOsO_6 (−74 K) and perhaps caused by the fact that the Pr^{3+} and Os^{5+} magnetic sublattices are interacting in a ferromagnetic-like manner. The high-field scans of Figure 6 support this conclusion and show ferromagnetic-like behavior down to the lowest temperatures. The transition is clearly seen and appears to signal magnetic coupling between Os^{5+} and Pr^{3+}. To evaluate whether similar magnetic coupling is observed also for other magnetic rare earth cations, the slightly more magnetic Nd^{3+} was also prepared in this double perovskite structure and its magnetization was studied.

Nd_2NaOsO_6. The temperature dependence of the magnetization for Nd_2NaOsO_6 in an applied field of 10, 15, 20, 30, and 40 kG is shown in Figure 8. The plot shows an increase in the magnetization up to ~20 K, where at fields of 20 kG and less, it reaches a maximum. At lower temperatures and fields of less than 20 kG, it makes an

(45) Lufaso, M. W.; Woodward, P. M. *Acta Crystallogr.* **2001**, *B57*, 725.
(46) Shannon, R. D. *Acta Crystallogr.* **1976**, *A32*, 751.
(47) Goldschmidt, V. M. *Geochemische Verteilungsgesetze der Elementer V11*; Naturvidenskaplig Klasse: Oslo, 1926.
(48) Gemmill, W. R.; Smith, M. D.; Mozharivskyj, Y. A.; Miller, G. J.; zur Loye, H.-C., in preparation.

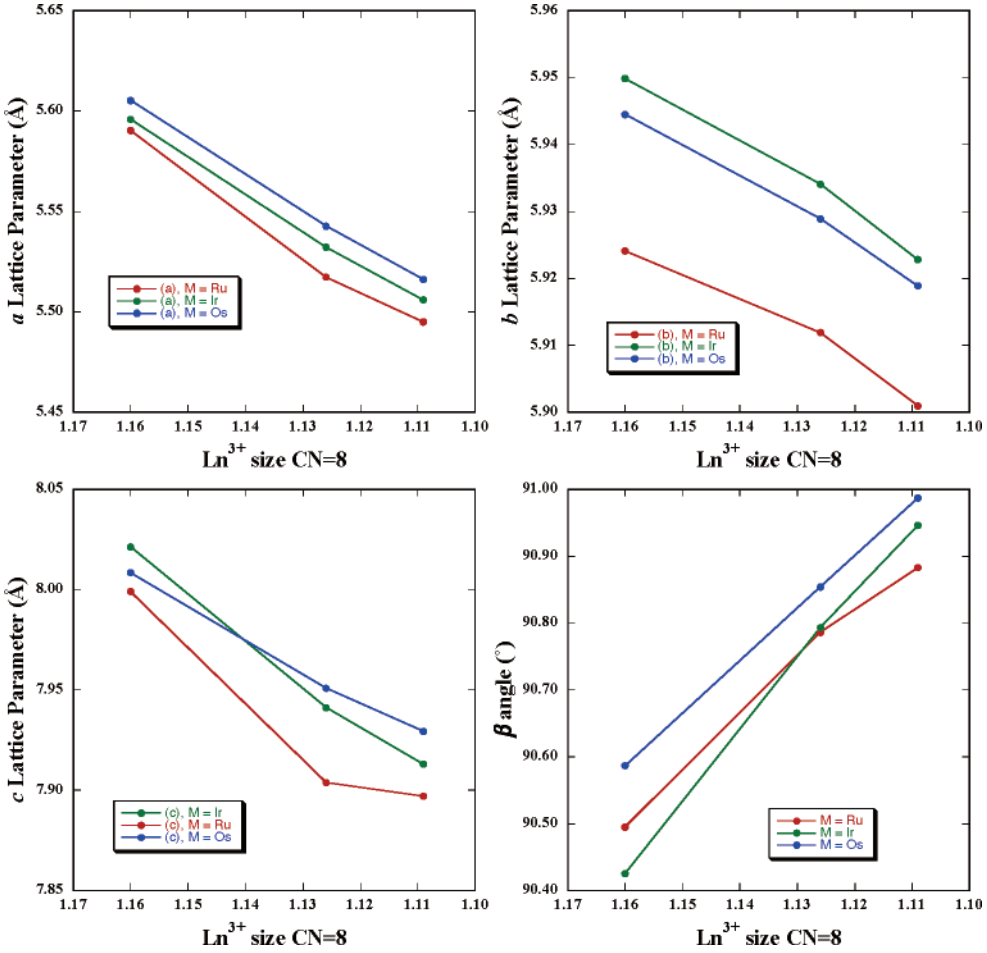

Figure 3. Variation of the lattice parameters and β angle as a function of Ln^{3+} size (CN = 8) for the three series of double perovskites Ln_2NaMO_6 (Ln = La, Pr, Nd; M = Ru, Ir, and Os),[34,36] where red = Ru, green = Ir, and blue = Os.

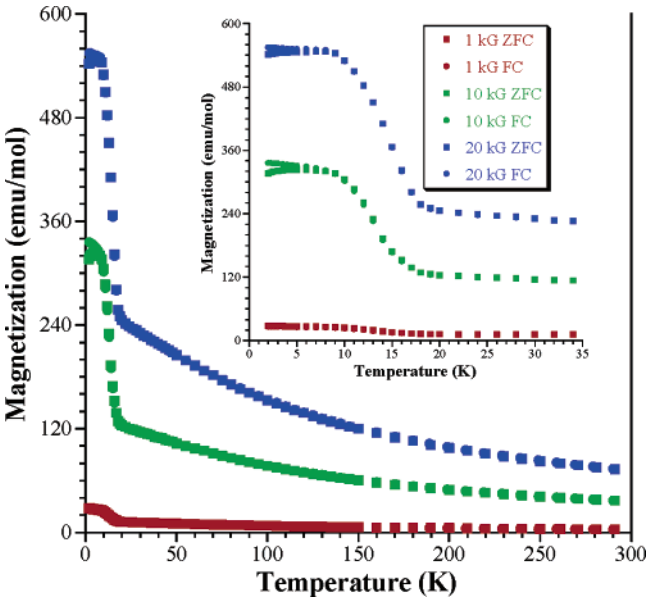

Figure 4. Temperature dependence of the magnetization of La_2NaOsO_6 in applied fields of 1, 10, and 20 kG.

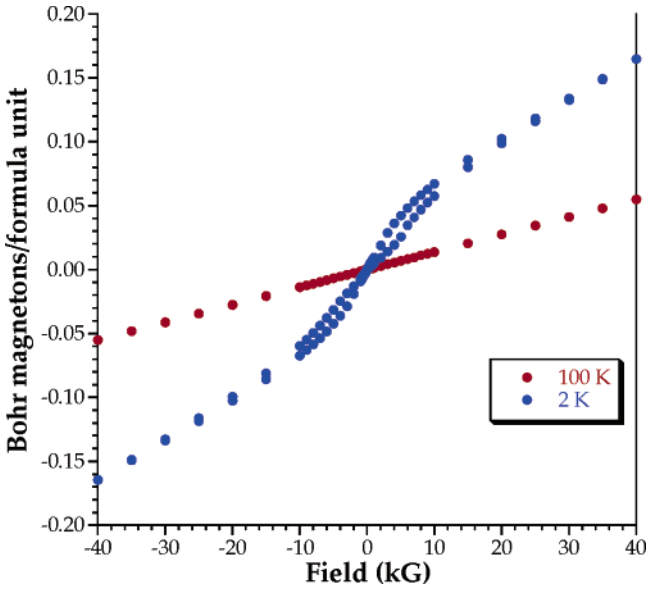

Figure 5. Field dependence of the magnetization of La_2NaOsO_6 measured at 100 and 2 K.

antiferromagnetic-like downturn followed by another anomaly at ~10 K and continues down to a minimum at the lowest measured temperature of 2 K. The 20 kG data exhibit an increase in the susceptibility at ~10 K (see inset Figure 8). At fields above or at 30 kG, the magnetization undergoes a ferromagnetic-like increase at ~20 K and eventually reaches a maximum at the lowest measured temperature of 2 K. Fitting the high-temperature susceptibility of the 10 kG zfc

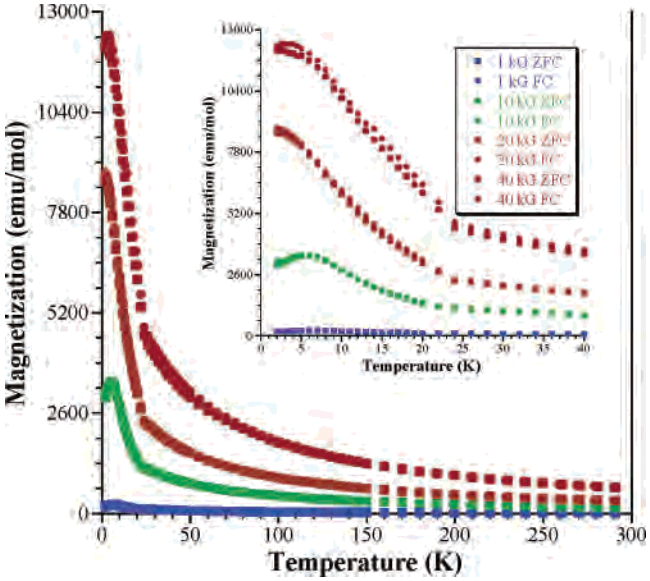

Figure 6. Temperature dependence of the magnetization of Pr_2NaOsO_6 in applied fields of 1, 10, 20, and 40 kG.

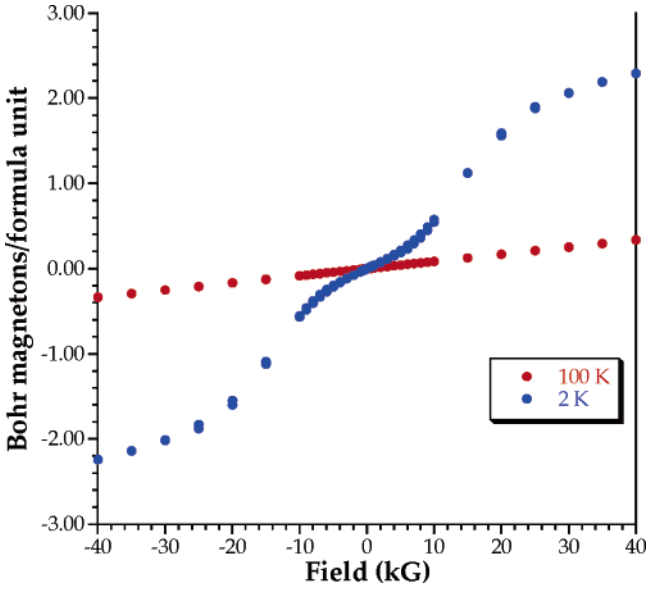

Figure 7. Field dependence of the magnetization of Pr_2NaOsO_6 measured at 100 and 2 K.

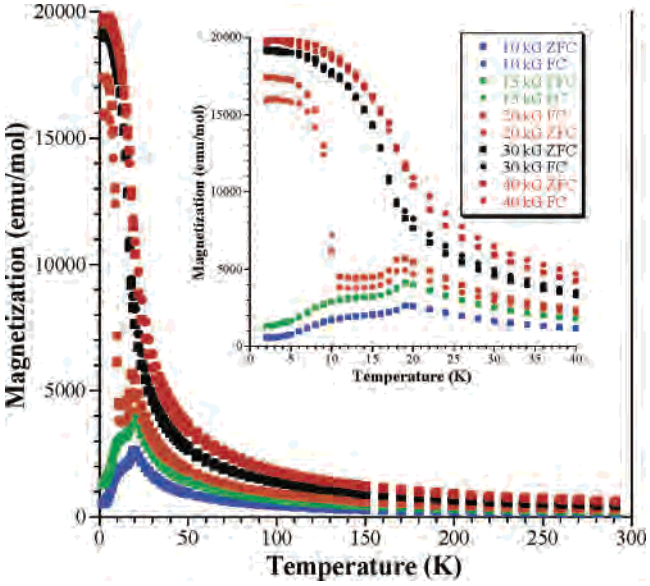

Figure 8. Temperature dependence of the magnetization of Nd_2NaOsO_6 in applied fields of 10, 15, 20, 30, and 40 kG.

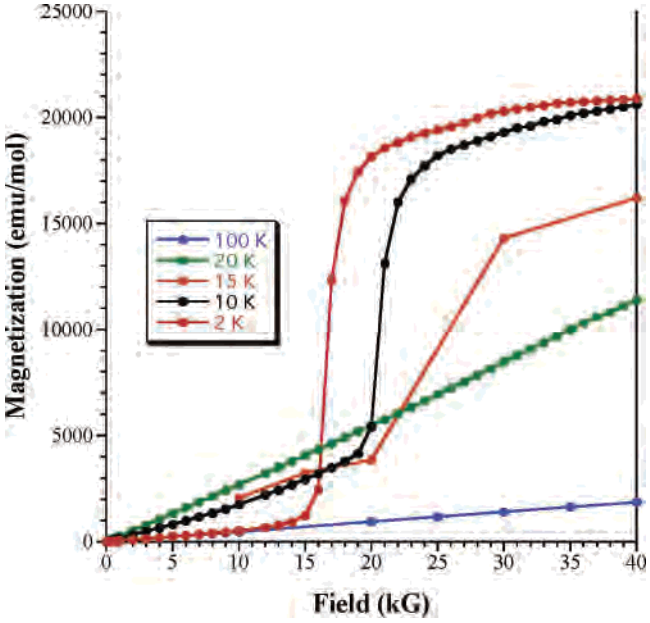

Figure 9. Field dependence of the magnetization of Nd_2NaOsO_6 measured at 2, 10, 15, 20, and 100 K. Lines are present to connect dots and to guide the eye. (The 15 K data were obtained from magnetization values at 15 K for the zfc data sets shown in Figure 8 for 10, 15, 20, 30, and 40 kG.)

data ($100 < T < 300$) to the Curie−Weiss law (see above) results in values of $\mu_{eff} = 6.00\ \mu_B$, $C = 4.50$ emu/K mol^{-1}, $\theta = 3$ K, which agrees reasonably well with the theoretical value (6.42 μ_B). Unlike for Pr_2NaOsO_6, the measured moment of 6.00 μ_B agrees with the calculated moment (6.07 μ_B) obtained when the Os(V) moment from La_2NaOsO_6 is used to determine the theoretical moment. Figure 9 shows the field dependence of the positive magnetization (0−40 kG) recorded at 2, 10, 15, 20, and 100 K. The overall picture demonstrates a very clear and sharp spin-flop transition between 15 and 20 kG, where for lower measurement temperatures the spin-flop transition occurs at lower applied fields, ∼15 kG at 2 K, ∼20 kG at 10 K, and 25 kG at 15 K.

Magnetic Phase Diagram. The *H* versus *T* phase diagram for Nd_2NaOsO_6 is shown in Figure 10 and depicts the multiple magnetic transitions in Nd_2NaOsO_6 and illustrates how both applied field and temperature induce different magnetic states in this material. The PM-AFM1/FM and the AFM1-AFM2 boundaries were determined from the temperature dependence of the magnetization data, that is, Figure 8; the lines mark the approximate locations of the magnetic phase boundaries. Based on the temperature-dependent magnetization data, there appear to be two Néel temperatures, T_{N1} and T_{N2} at 20 and 10 K, respectively, marking the boundaries between the PM region above 20 K and the AFM1 region existing between 20 and 10 K, and the boundary between the AFM1 and the AFM2 regions existing below 10 K at fields below ∼17 kG. The dividing line separating the FM region from the AFM2 region was

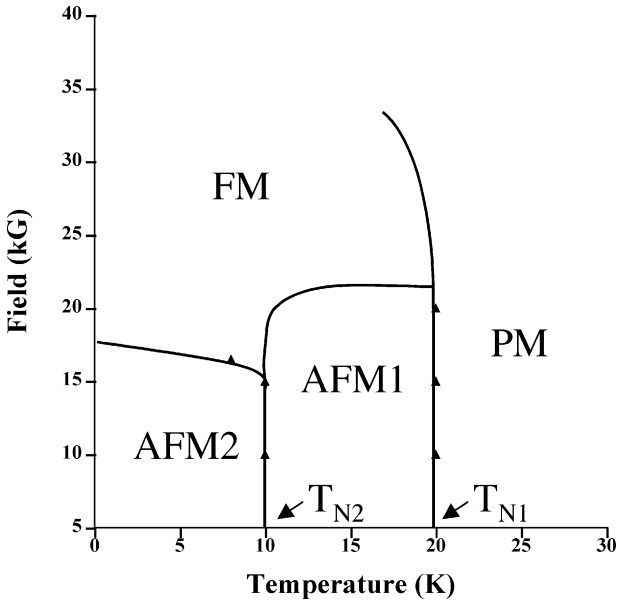

Figure 10. Magnetic phase diagram for Nd_2NaOsO_6. AFM = antiferromagnetic, FM = ferromagnetic, and PM = paramagnetic. The lines serve only as guides for the eyes.

determined from the field dependence of the magnetization at 10 K (Figure 9). It can be seen that the magnetization begins to increase at ~17 kG, which is attributed to a ferromagnetic state.

There is significant magnetic coupling between the A and B sites in these double perovskite osmates, which results in fairly complicated magnetic phase diagrams. In both Pr_2NaOsO_6 and Nd_2NaOsO_6, the magnetism at low temperatures is dominated by the rare earth cation. Only a limited number of double perovskites with rare earth cations on the A-site have been prepared, and, among them, it is rare to find such strong magnetic coupling between the A and the B cations. For example, in the previously studied Ln_2NaIrO_6 and Ln_2NaRuO_6, there is no evidence of such strong coupling. In the case of Ir^{5+}, which has a nonmagnetic ground state, one would not expect strong coupling. On the other hand, Ru^{5+}, d^3, could in theory couple magnetically with the rare earth cations. It is possible that the greater radial extend of the osmium versus the ruthenium *d*-orbitals favors these strong magnetic interactions in Pr_2NaOsO_6 and Nd_2NaOsO_6. An assessment of whether this represents a general trend for osmium will have to await the synthesis and magnetic characterization of additional Ln_2MOsO_6 double perovskites, which is currently in progress.

Summary

The series of double perovskites Ln_2NaOsO_6 (Ln = La, Pr, Nd) was prepared as single crystals, and their magnetic properties were investigated. This is the first report on these osmates, and the growth of these oxides from molten hydroxide fluxes further establishes these melts as a successful solvent system for the preparation of oxide structures containing both lanthanides and platinum group metals. All three compounds show evidence for antiferromagnetism at low temperatures and low applied fields; however, a spin-flop transition to a ferromagnetic state occurs at fields of about 10 and 15 kG for Pr_2NaOsO_6 and Nd_2NaOsO_6, respectively, at a temperature of 2 K.

Acknowledgment. Financial support for this research was provided by the National Science Foundation through the grant DMR: 0134156 and by the Department of Energy through grant DE-FG02-04ER46122.

Supporting Information Available: Additional structural and crystallographic data. This material is available free of charge via the Internet at http://pubs.acs.org.

IC048637X